Lab on a Chip

Miniaturisation for chemistry, biology & bioengineering

www.rsc.org/loc

Volume 9 | Number 6 | 21 March 2009 | Pages 741–848

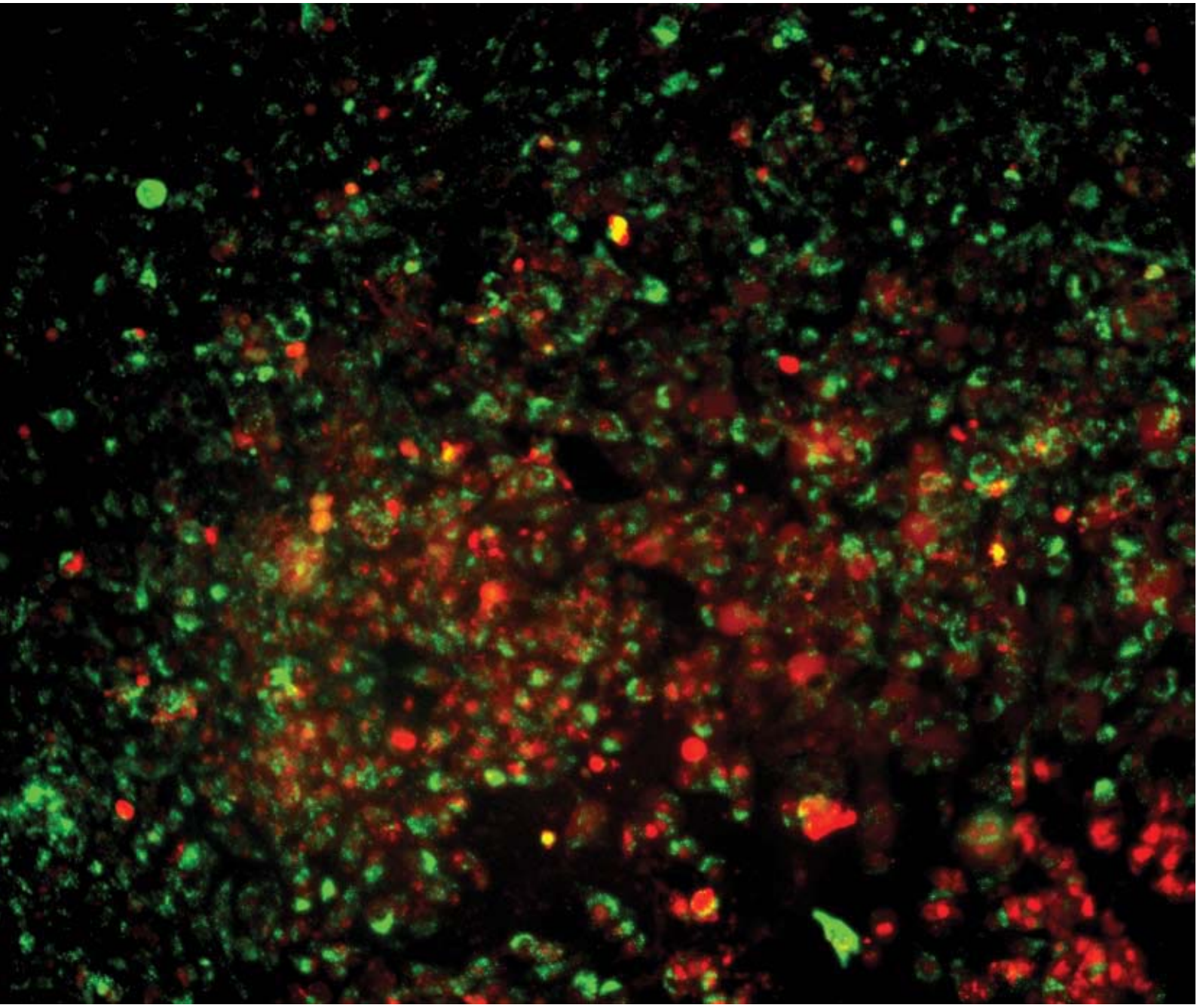

ISSN 1473-0197

RSC Publishing

Rapid generation of spatially and temporally controllable long-range concentration gradients in a microfluidic device†

Yanan Du,[ab] Jaesool Shim,‡[ab] Mahesh Vidula,[ab] Matthew J. Hancock,[ab] Edward Lo,[ab] Bong Geun Chung,[ab] Jeffrey T. Borenstein,[c] Masoud Khabiry,[ab] Donald M. Cropek[d] and Ali Khademhosseini*[ab]

Received 15th September 2008, Accepted 13th November 2008
First published as an Advance Article on the web 10th December 2008
DOI: 10.1039/b815990d

The ability to rapidly generate concentration gradients of diffusible molecules has important applications in many chemical and biological studies. Here we established spatially and temporally controllable concentration gradients of molecules (*i.e.* proteins or toxins) in a portable microfluidic device in an easy and rapid manner. The formation of the concentration gradients was initiated by a passive-pump-induced forward flow and further optimized during an evaporation-induced backward flow. The centimeter-long gradients along the microfluidic channel were shown to be spatially and temporally controlled by the backward flow. The gradient profile was stabilized by stopping the flow. Computational simulations of this dynamic process illustrated the combined effects of convection and diffusion on the gradient generation, and fit well with the experimental data. To demonstrate the applications of this methodology, a stabilized concentration gradient of a cardiac toxin, alpha-cypermethrin, along the microchannel was used to test the response of HL-1 cardiac cells in the micro-device, which correlated with toxicity data obtained from multi-well plates. The approach presented here may be useful for many biological and chemical processes that require rapid generation of long-range gradients in a portable microfluidic device.

Introduction

Concentration gradients of diffusible molecules (chemical compounds or biomolecules) play an important role in many chemical processes (*e.g.* crystal growth) as well as biological phenomena (*e.g.*, chemotaxis, morphogenesis and wound healing).[1–7] A variety of approaches have been developed for generating gradients of diffusible molecules driven either purely by diffusion or by a balance of convection and diffusion. Most of the existing approaches for gradient generation are diffusion-driven,[8] which can be generally categorized into: (1) forming gradients perpendicular to parallel laminar flows of varying concentrations[9–13] and (2) forming gradients along a channel by free-diffusion between a source and a sink.[14,15] The first method is advantageous for producing stable complex gradients, but the experiments are not compatible with non-adherent and weakly adherent cells and the shear/drag force generated by the flow may alter the intercellular signaling pathways. Moreover, to generate the laminar flows, pumping systems with external connections (*i.e.* tubing and valves) are often used, which limit the portability and ease of use of the device.[16] To maintain a continuous flow, relatively large volumes of fluid containing the materials of interests are consumed, which constrain their applications for precious materials (*i.e.* growth factors, drugs). The second approach normally requires larger gradient generation times and the gradient produced is hard to maintain over long time periods.[17] Gradients have also been formed parallel to the direction of flow. Goulpeau *et al.* built up longitudinal concentration gradients along their microchannel by using transient dispersion along the flow.[18] Kang *et al.* developed a device that generated concentration gradients parallel to the direction of flow by using a convective–diffusive balance in a counter-flow configuration.[19] Although these approaches could be used to rapidly generate concentration gradients in less than 1 min, they still required external components *i.e.* hydrostatic pumps or valves to introduce and control the flows within the channels.

The ability to build pumpless fluidic devices that generate controllable gradients while maintaining the portability and scalability of microfluidic systems is of significant benefit for field testing and high-throughput studies. Furthermore, the ability to generate longer gradients can be used to test the effects of molecular dose responses on cell behaviors. One approach to eliminate the use of external pumps is by using a passive-pump technology, which was first developed by Walker *et al.* as a semi-autonomous method for pumping fluid. Passive-pump technology only requires a device capable of producing small

[a]*Center for Biomedical Engineering, Department of Medicine, Brigham and Women's Hospital, Harvard Medical School, Boston, MA, 02115, USA. E-mail: alik@mit.edu; Fax: +1 617-768-8477; Tel: +1 617-768-8395*
[b]*Harvard-MIT Division of Health Sciences and Technology, Massachusetts Institute of Technology, Cambridge, MA, 02139, USA*
[c]*Draper Laboratory, Cambridge, MA, 02139, USA*
[d]*U.S. Army Corps of Engineers, Construction Engineering Research Laboratory, Champaign, IL, 61822, USA*

† Electronic supplementary information (ESI) available: Input parameters for the computational simulations; calculation of the volumetric flow rate of the forward flow driven by the passive-pump; calculation of the volumetric flow rate of the backward flow induced by evaporation; effect of diffusion on the change of the gradient profile; cytotoxicity testing of alpha-cypermethrin on HL-1 cells cultured in 96-well microplate and supplementary videos. See DOI: 10.1039/b815990d

‡ Present address: School of Mechanical Engineering, Yeungnam University, Gyeongsan-si, Gyeongsanbuk-do, Korea.

drops of liquid, such as a pipette.[16,20] The surface tension difference between the larger drop of solution at the outlet and the smaller drop of solution at the inlet was used to pump the small drop of liquid through the microchannel, which has been shown to be a powerful high-throughput microfluidic tool for cell culturing. Evaporation has also been used as the driving force in 'pump-less' microfluidic devices. Evaporation is a well-known issue when handling small liquid volumes, especially in microfluidic devices.[21,22] While the loss of volume due to evaporation may cause unwanted effects such as the change of concentrations or osmolarity of the fluid solution; evaporation in microfluidic devices has proven to be a useful tool in several applications, including generating slow, steady flows in microchannels used for chromatography,[23] DNA analysis devices,[24] and sample concentration.[25,26]

In this study, we take advantage of a reversed flow induced by the passive-pump and evaporation-driven sequence to rapidly establish centimeter-long concentration gradients of molecules along the channel of a simple and portable microfluidic device. We applied the passive-pump technology to generate a forward flow from the inlet to the outlet of the channel, which introduced the molecules of interest (with volume less than 10 μL) into the microfluidic device in a rapid and simple manner and initiated a concentration gradient profile of the molecules due to the parabolic shape of the front flow. An evaporation-induced backward flow from the outlet to the inlet of the channel followed the forward flow, which resulted in the formation of dynamic concentration gradients of the molecule. The centimeter-long concentration gradients were in parallel with the flow direction along the microfluidic channel, which could be spatially and temporally controlled; and a particular gradient profile could be stabilized by stopping the flow.

Our approach to generate a concentration gradient mainly relies on the flow properties and the combined effect of convection and diffusion. Throughout the channel the flow is essentially fully developed laminar Poiseuille flow in a rectangular channel, a textbook example where the Navier–Stokes equations admit an exact solution [*e.g.* ref. 27, eqn 3–48, pp 120].[27] The Peclet numbers for the forward and backward flows are approximately 1000 and 10, respectively. In the axial direction, the chemical transport is mainly due to convection; since the flow is essentially axial, the transport in the transverse direction is mainly due to molecular diffusion. This type of chemical spreading, involving both axial convection and transverse molecular diffusion, is called Taylor dispersion.[28–30] Theoretical descriptions of dispersion in microchannels are well developed.[13,18,31,32] Much of the existing theory for dispersion assumes steady flow. While the flows due to the passive-pump and evaporation stages are approximately steady, the transition between the two (flow reversal) is not. We have thus numerically solved for the flow and chemical concentration.

Computational simulations of the gradient generation and stabilization agree well with the experimental data, which show that the concentration gradients are mainly generated and controlled by a combined effect of convection (forward and backward flow) and molecular diffusion. We demonstrate an application of this portable microfluidic device for rapid concentration gradient generation by conducting a cytotoxicity test. A stabilized concentration gradient of a cardiac toxin was used to test the toxicity response of HL-1 cardiac cells seeded within the channel. Given its ease of use, portability, low consumption and scalability, this approach may be useful for various biological and chemical processes for rapid generation of long-range gradients.

Experimental

Materials

All the reagents were purchased from Sigma-Aldrich (St. Louis, MO), unless specifically mentioned.

Fabrication of the microfluidic device

The microfluidic device was fabricated by using standard soft-lithography methods. Photomasks with channel patterns were designed using AutoCAD and printed on transparencies with 20 000 dpi resolution (CAD/Art Services, Inc., Bandon, OR). Master molds patterned with 100 μm thick resist were made by patterning a negative photoresist (SU-8 2050, Microchem, MA) on a silicon wafer. PDMS molds were fabricated by curing prepolymer (Sylgard 184, Essex Chemical, Midland, MI) on silicon masters patterned with SU-8 photoresist. Briefly, PDMS molds were generated by mixing silicone elastomer and curing agent (10 : 1 ratio). The PDMS prepolymer was poured on the silicon master that was patterned with photoresist and cured at 70 °C for 2 h. PDMS molds were then peeled off from the silicon wafer. The inlet and outlet of the microchannel were created by a sharp punch (hole radius: 0.4 mm) for medium perfusion and cell seeding. The microfluidic device consisted of a top PDMS fluidic channel and a bottom glass slide. The top fluidic channel was 100 μm (height) × 50 mm (length) × 1.6 mm (width), which was bonded to the bottom glass slide after treatment by oxygen plasma (Harrick Scientific, Pleasantville, NY).

Generation and stabilization of the concentration gradient

The channel was initially filled with Dulbecco's Phosphate Buffered Saline (DPBS, Gibco, Carlsbad, CA). A 200 μL drop of DPBS was pipetted onto the outlet opening and a 2 μL drop of DPBS containing the molecule of interest was dropped onto the inlet opening and subsequently entered the channel automatically. After the small drop entered the channel completely, a second drop containing 2 μL was pipetted onto the inlet to continue the forward flow. If the inlet was not refilled, the forward flow would stop and a backflow would occur due to evaporation at the room humidity (~30%). To visualize the dynamic process of the concentration gradient generation, fluorescein isothiocyanate-dextran (FITC-Dextran, molecular weight (MW): 10 kD) was used as the model molecule, and the fluorescence image series was captured using a Kodak Gel Logic 100 Imaging System. The average fluorescence intensity along the whole channel was quantified by ImageJ software. To stabilize the concentration gradient, the evaporation-driven flow was stopped by either sealing the inlet with a drop of mineral oil or putting the microfluidic device into an enclosure with 100% humidity.

Computational model

Computational fluid dynamics was used to simulate the dynamic process of concentration gradient generation using the finite element method (COMSOL Multiphysics v3.2, Burlington, MA). Unstructured mesh generation method was performed and 5420 elements were used for constructing the 3D mesh domain. The concentration gradient generation driven by the passive-pump and evaporation fluid model was based on the following three equations, including the 3D incompressible Navier–Stokes equations (*i.e.* the momentum and continuity equations):

$$\rho\left(\frac{\partial u}{\partial t} + (u \cdot \nabla)u\right) = -\nabla p + \mu\nabla^2 u \quad (1)$$

$$\nabla \cdot u = 0 \quad (2)$$

and the convection–diffusion transport equation:

$$\frac{\partial C}{\partial t} + (u \cdot \nabla)\, C = D\nabla^2 c \quad (3)$$

where ρ, u, and p are the density, flow velocity and pressure of the liquid, and C and D are the concentration and diffusivity of the molecules in the liquid. At each time step, the flow u is first found independently of the concentration, which is then found using the computed flow. The boundary conditions are as follows. At the inlet, the flow velocity was set to 0.08 cm s^{-1} for the forward flow and 10.1 μm s^{-1} for the backward flow. These values agree with the average flow rates produced by the passive-pump and by evaporation, experimentally observed and analytically calculated (see ESI).† At the outlet we imposed zero normal stress, and at the channel walls we imposed the no-slip conditions ($u = 0$). For the convection–diffusion equation, constant concentration was set at the channel inlet and zero concentration at the channel outlet. No-flux conditions were imposed at all channel walls ($\partial C/\partial n = 0$). Table 1 in the ESI† summarizes the input parameters used for the numerical simulations. The channel geometry was set as 5 cm × 1600 μm × 100 μm and FITC-Dextran was used as the model dye molecule. To quantify the simulation results with time, the concentrations were extracted from the centerline along the channel and normalized with the maximum concentration at the inlet of the channel.

Cytotoxicity testing

HL-1 cells (cardiac muscle cell line) were cultured with medium containing 87% Claycomb medium, 10% fetal bovine serum (FBS), 1% penicillin/streptomycin, 1% norepinephrine and 1% L-glutamine at 37 °C in a humidified 5% CO_2/95% air incubator, which were generously provided by Dr William Claycomb, Louisiana State University. To enhance the cell adhesion, the bottom glass slide was coated with a mixture of extracellular matrix (0.02% gelatin (w/w) and 5 μg mL^{-1} fibronectin) after the top channel was bonded to the bottom glass slide. To seed the cells into the microfluidic device, the cells were trypsinized and seeded through the outlet port using dynamic seeding at a cell density of 2×10^6 cells mL^{-1} that allowed uniform cell distribution. Cells were cultured for 2 h to ensure attachment. The medium was then changed and three drops of 2 μL medium containing 20 mM alpha-cypermethrin were introduced by passive-pumping and a concentration gradient was established by leaving the microfluidic device in the hood for 5 min to allow for evaporation-induced backflow. The microfluidic device was then transferred to a humidified incubator where the concentration gradient of the toxin was stabilized and the cells were treated for 4 h. Cell morphology and viability was characterized by peeling off the top channel and incubating the cells with live/dead dyes (2 μL calcein AM and 0.5 μL ethidium homodimer-1, Molecular Probes, CA) in 1 mL DPBS for 10 min. ImageJ was used to quantify the fluorescence images of live-dead staining of the cells. At least three images were used for quantification of the cell viability.

Results

Generation of the concentration gradient by passive-pump-induced forward flow and evaporation-induced backward flow

We aimed to generate a stable concentration gradient by using the process shown in Fig. 1. The microfluidic channel was initially filled with DPBS, and a 200 μL drop of DPBS was pipetted onto the outlet. A small drop of 2 μL DPBS containing FITC-Dextran was then dropped onto the inlet (Fig. 1A) and entered the channel automatically due to the differential surface tensions between the drops (Fig. 1B). After the small drop entered the channel completely, a second drop was pipetted onto the inlet to continue the forward flow. In our current microfluidic device setup, three drops were sufficient for the fluid to reach the outlet end of the 5 cm-long channel (Fig. 2A). The forward flow rate was ~1 mm s^{-1} as measured experimentally and calculated analytically (see ESI).† Therefore, approximately 1 min was required to introduce three drops of solution containing the fluorescent dye into the channel *via* the forward flow. Following the forward flow, a backward flow was induced by the evaporation of the solution from the inlet.[25] We observed the formation of a dynamic concentration gradient of the fluorescent dye along the channel, which was parallel to the backward flow and moving backward to the inlet (Fig. 1C and Fig. 2B and Video 1 in

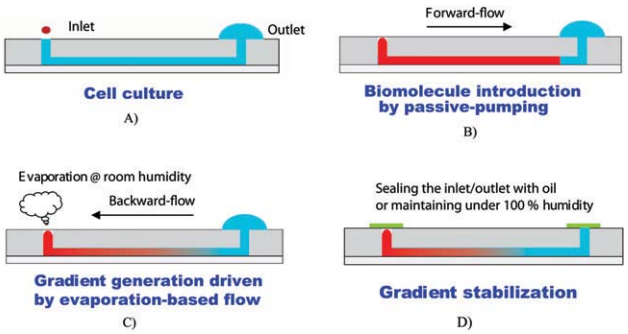

Fig. 1 Schematic of the gradient generation and stabilization process: A) Microfluidic channel was first filled with DPBS (or culture medium); a large drop was placed on the outlet opening and a small drop containing diffusible molecules was pipetted on the inlet opening; B) solution was introduced into the channel automatically by the passive-pump-induced forward flow; C) a concentration gradient of molecules was generated during the evaporation-based backward flow; D) the gradient profile could be stabilized by stopping the evaporation, either by sealing the inlet with mineral oil or by maintaining the microfluidic device at 100% humidity.

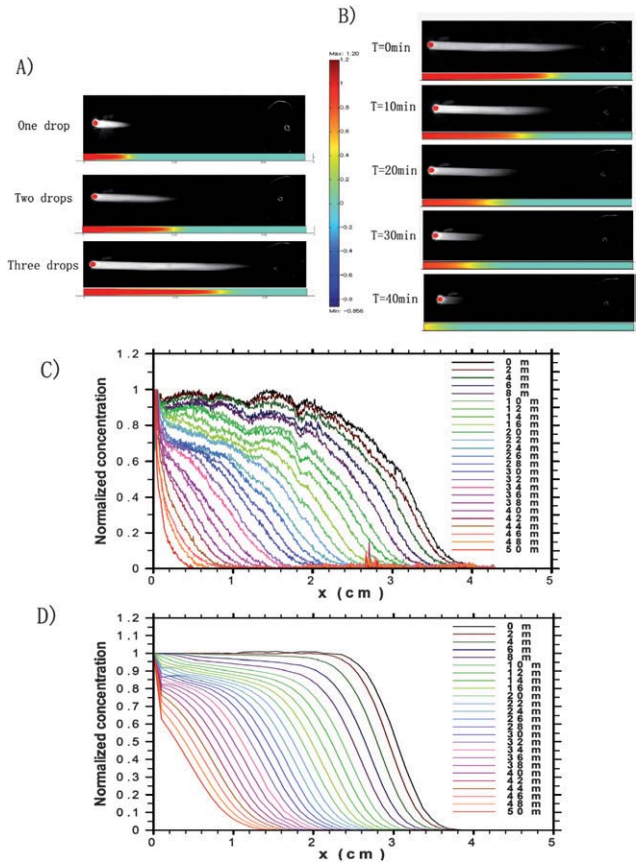

Fig. 2 Experimental and simulation results of dynamic gradient generation in the microfluidic channel: A) Fluorescence images, extracted from a video clip, showing the forward flow of a solution containing FITC-Dextran into the microfluidic channels by using a passive-pump. The corresponding simulation results obtained by the finite element method are positioned directly below each experimental fluorescence image. The vertical color scale denotes fluorescence intensity. B) Fluorescence images, extracted from a video clip, demonstrating the generation of a dynamic gradient of FITC-Dextran by using an evaporation-driven backward flow. The corresponding simulation results obtained by finite element method are positioned below the experimental image. Experimental C) and simulation D) results showing the normalized fluorescence signal of FITC-Dextran along the channel at different times during the backward flow.

ESI).† The backward flow rate was 10.1 μm s^{-1} as measured experimentally and calculated analytically (see ESI),† which was significantly slower than the forward flow. The evolution of the centimeter-long concentration gradient that formed along the channel during the 50 min backward flow was quantified by measuring the fluorescent intensity along the channel (Fig. 2C), which was assumed to be proportional to the concentration of the fluorescent molecules. During the backward flow, the fluorescent dye and the concentration gradient moved backward toward the inlet, and the gradient steepened.

Simulation of the dynamic gradient generation

We used a finite element method to simulate the dynamic process of concentration gradient formation, which could be separated into two stages: a forward flow stage and a backward flow stage (see ESI, Videos 2 and 3).† To mimic the concentration distribution due to the three drops added at the inlet during the forward flow stage, the final concentration from the previous droplet was used as the initial concentration for the next droplet added. Top views of the simulated concentration profiles after the addition of one, two and three drops, agree with the experiment results (Fig. 2A). The final concentration distribution of the three-drop forward flow stage was used as the initial concentration for the simulation of the backward flow stage. Top views of the simulated concentration distribution at different times in Fig. 2B demonstrate the formation of the dynamic concentration gradient during backward flow, which agrees with the experimental results. The simulated normalized concentration during the backward flow stage (Fig. 2D) followed a similar trend to the experimental data (Fig. 2C).

The gradient is generated by dispersion, the combined effect of convection and molecular diffusion, and flow reversal, which changes the direction of the parabolic flow (Fig. 3A). Concentration distributions at different locations along the channel at

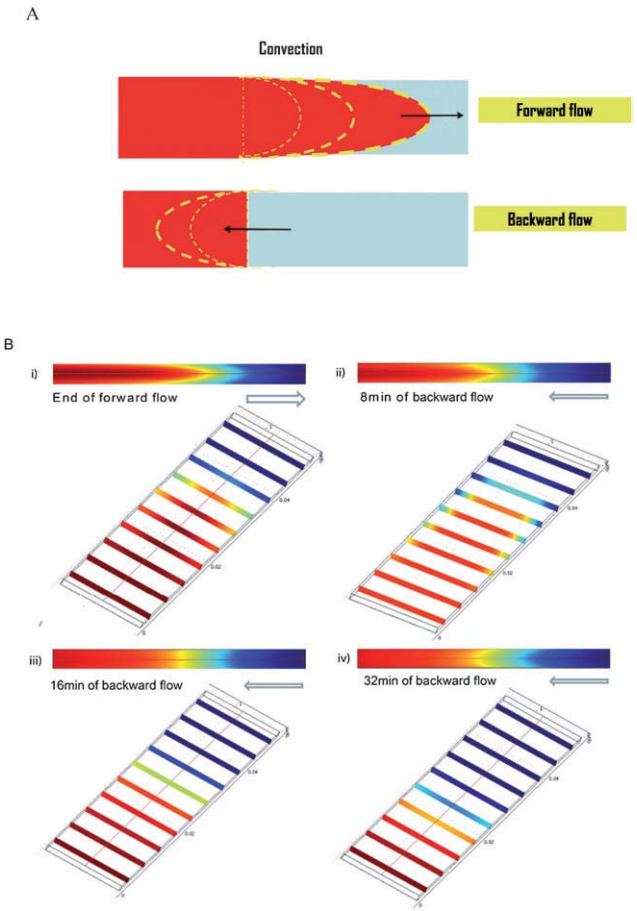

Fig. 3 Mechanism of gradient generation by dispersion (convection and diffusion): A) effect of flow reversal on concentration gradient; B) simulation results to verify the effects of dispersion on the formation and dynamic change of the concentration gradient: top-down and cross-sectional views of the simulation results of the concentration profiles at i) the end of forward flow, ii) 8 min, iii) 16 min, and iv) 32 min after the backward flow.

different times are shown in Fig. 3B. The rapid forward flow generates a parabolic concentration profile (Fig. 3B i). The backward flow then gradually flattens the parabolic profile and renders the concentration distribution laterally uniform (Fig. 3B ii). A centimeter-long concentration gradient with uniform cross-sectional distribution is formed after 16 min of backward flow for a molecule with a diffusivity of 1.7×10^{-6} cm^2 s^{-1} (*i.e.* FITC-Dextran) (Fig. 3B iii). As the backward flow continues, the concentration forms a slightly inverted parabolic profile. However, since the backward flow is significantly slower than the forward flow, the uniformity of the concentration distribution was not significantly affected, and a relatively uniform concentration gradient moved backward toward the inlet (Fig. 3B iv).

The timescale for molecular diffusion across a distance L is $L^2/(\pi^2 D)$, where D is the molecular diffusivity. The timescales for vertical and horizontal mixing of FITC-Dextran across the 100 μm height and 1.6 mm width of the channel are therefore 6 s and 25 min, respectively. Thus, the chemical concentration is essentially uniform vertically across the microchannel, and it suffices to consider only its horizontal variation, as we have done. The timescale for molecular diffusion across the width of the channel is significantly greater than the duration of the forward flow and commensurate with the timescale of the backward flow. It is therefore instructive to consider the role of the backward flow on gradient generation. After a concentration profile was produced by the forward flow, we compared the concentration profiles obtained after a given duration of backward flow with those obtained instead from the same duration of pure diffusion. The results indicate that the main role of backward flow is to spatially place the gradient. Moreover, the backward flow slightly elongates the gradient by 1–10% (see ESI).†

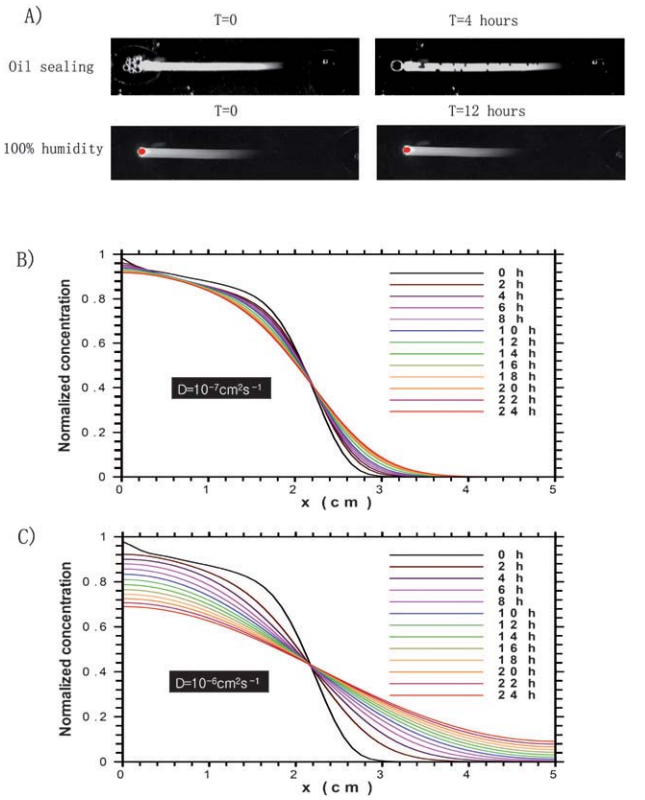

Fig. 4 Evolution of the concentration gradient profile due to molecular diffusion: A) FITC-Dextran in the microfluidic channel for 4 h with flow stopped by oil sealing (top) and for 12 h with flow stopped by maintaining a 100% humidity environment (bottom); B, C) Simulation results of the dynamic concentration gradient driven by molecular diffusion over one day: B) molecules with diffusivity of 10^{-7} cm^2 s^{-1}, C) molecules with diffusivity of 10^{-6}cm^{2}s^{-1}.

Stabilization of the concentration gradient

To achieve the spatial and temporal control of the dynamic concentration gradients, a particular concentration gradient was stabilized using two methods to stop the flow. As shown in Fig. 1D and Fig. 4A, evaporation from the inlet was prevented either by sealing with mineral oil or by placing the microfluidic device in an environment with 100% humidity (water bath or cell incubator). The oil sealing approach could stabilize a particular concentration gradient profile for up to 4 h before evaporation through the PDMS layer became noticeable (indicated by the small cavities in the fluorescence image in Fig. 4A), while a concentration gradient profile could be stabilized under 100% humidity for at least 12 h.

By preventing evaporation, the flow is stopped and spreading is due purely to (passive) molecular diffusion. The evolution of the concentration profile due only to molecular diffusion is shown over one day in Figs. 4B and 4C. The flow was terminated by setting equal the pressures at both the inlet and outlet of the channel. The concentration gradient after 12 min of backward flow was used as the initial concentration profile. Simulations were run for two types of molecules with diffusion coefficients differing by an order of magnitude. The simulation results indicate that for large molecules with small diffusion coefficients (*e.g.* 10^{-7}cm^2 s^{-1}), little change in the concentration gradient occurs due to molecular diffusion after one day. For smaller molecules with larger diffusion coefficients (*e.g.* 10^{-6}cm^2 s^{-1}), the effect of molecular diffusion on the concentration gradient profile became evident after 6 h and approached equilibrium throughout the channel within one day.

Estimates can be made of the timescale over which the gradient is maintained, since exact analytical solutions are known for the diffusion equation for any initial concentration gradient. The exact solutions decay exponentially with rate constants approximately equal to $\pi^2 D/L^2$, where L is the length scale of the concentration gradient and D is the molecular diffusivity. The concentration gradient is maintained to within 10% of its initial state over a time interval of $0.1L^2/(\pi^2 D)$ (see ESI).† Centimeter-long concentration gradients of chemicals with molecular diffusivities of 10^{-7}cm^2 s^{-1} and 10^{-6}cm^2 s^{-1} remain within 10% of their initial states over time intervals of approximately 28 h and 2.8 h, respectively. These results indicate that stable concentration gradients can be maintained for molecules over a wide range of diffusion coefficients for several hours.

Stabilized concentration gradient for cytotoxicity testing

To exhibit the potential applications of the spatially and temporally controllable concentration gradient, we utilized the stabilized concentration gradient technique for cytotoxicity

testing. A cardiac muscle cell line (HL-1)[33] was used to investigate the cytotoxicity of alpha-cypermethrin, a cardiac toxin.[34] Three drops of 2 μL medium containing 20 mM alpha-cypermethrin were loaded consecutively into the micro-devices with HL-1 cells seeded along the channel. A concentration gradient of the toxin was established by evaporation when the micro-device was left at ambient conditions for 5 min (5 min exposure does not cause severe damage to cell viability, see ESI)† and this gradient was stabilized when the micro-device was transferred to the humidified incubator. HL-1 cells exposed to the toxin concentration gradient for 4 h exhibited distinguishable morphologies along the channel, with more severe effects observed in the regions containing higher concentrations of toxin (Fig. 5A). The drastic morphological change of HL-1 cells exposed to various concentrations of toxin was also observed when the cytotoxicity testing was conducted with HL-1 cells seeded in a 96-well plate (see ESI).† We further tested the cytotoxicity of the toxin gradient on the HL-1 cells by conducting a live-dead assay.

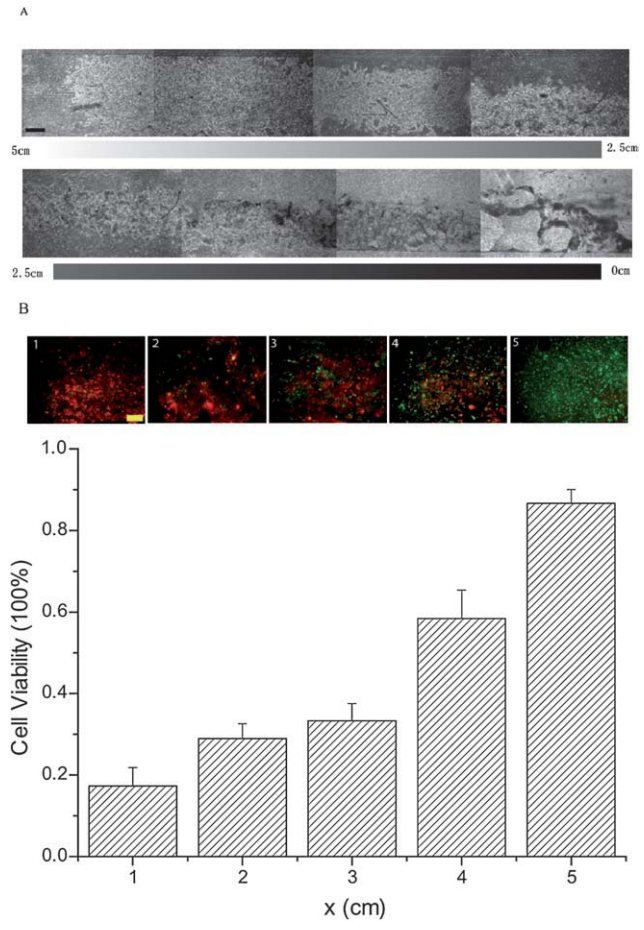

Fig. 5 Toxicity of a stabilized concentration gradient of alpha-cypermethrin on the HL-1 cells from outlet (5 cm) to inlet (0 cm) after 4 h residence time: A) Phase contrast images to show the morphology of the HL-1 cells along the 5 cm-long microfluidic channel after treatment with the toxin concentration gradient (scale bar: 600 μm); B) Representative fluorescent images (above) and their quantification (below) characterize the viability of HL-1 cells along the 5 cm-long microfluidic channel after treatment with the toxin concentration gradient. (Scale bar: 400 μm).

A correlation of cell viability was found with the toxin concentration gradient along the channel (Fig. 5B). According to the correlation between cell viability and morphology changes with respect to alpha-cypermethrin concentration obtained from the toxicity testing on HL-1 cells seeded in 96-well plates, the experimental conditions used here established a concentration gradient of the toxin from 12.5 to 0 mM along the 5 cm-long channel based on the assay conducted in this study.

Discussion

The goal of the present study is to develop a simple and rapid approach for long-range concentration gradient generation in a portable microfluidic device. Several features of the current approach for concentration gradient generation distinguish it from existing methods: 1) the gradient is generated by dispersion, the combined effect of convection and molecular diffusion, and flow reversal, which changes the direction of the parabolic flow; 2) due to its convection-driven nature, the process of gradient generation was rapid (within several minutes), highly dynamic (throughout the backward flow stage) and spatially/temporally controllable (by controlling the evaporation-induced backflow); 3) the gradient can be formed by consuming low amounts of the molecule of interest (from 2–6 μL for the current microfluidic channel design); 4) centimeter-long concentration gradients can be generated parallel to the flow direction along the channel; and 5) the approach was simple and highly reproducible in a portable microfluidic device, requiring only a pipette for implementation.

The gradient generation process is highly reproducible at ambient conditions (*i.e.* 22 °C, 30% relative humidity). Variations in temperature and humidity in the laboratory mainly affect the gradient generation process by slightly altering the backward flow rate induced by evaporation (see ESI);† their effects on the forward flow and the diffusion of the molecule are negligible.

We asserted above that the flow is essentially fully developed Poiseuille flow throughout the rectangular channel. Regions of adjustment to the fully developed flow exist at the ends of the channel. However, based on the Reynolds numbers (0.1 and 0.001) of the forward and backward flows, the extent of these adjustment regions is short: approximately the channel height [ref. 27, pp. 114, eqn 3–28].[27] Thus, throughout the channel the flow is essentially fully developed Poiseuille flow.

The concentration gradient profile in our device can be easily altered and controlled by choosing the initial analyte concentration in the applied drops and by manipulating the timing of the forward and backward flow. Factors affecting the flow properties, such as the fluid viscosity, the pressure difference between the inlet and outlet, the rate of evaporation and the geometry of the microfluidic channel are expected to affect the gradient generation and are currently under investigation.

Conclusions

We achieved rapid generation of centimeter-long concentration gradients of molecules using a reversed flow in a simple and portable microfluidic device. The gradients along the microfluidic channel could be spatially and temporally controlled and stabilized. Computational simulations supporting the

experimental results indicate that dispersion (convection and molecular diffusion) and the flow reversal lead to dynamic gradient generation. In an example drug test, we applied a stabilized gradient of a cardiac toxin concentration to test the response of HL-1 cardiac cells. The cell morphology and viabilities exhibited drastic differences along the microchannel, which correlated to the concentration gradient of the toxin. We believe that this simple and rapid approach for gradient generation on a controllable centimeter-long scale is a promising platform for applications such as drug testing and studying biological phenomena, such as chemotaxis. This passive-pump based approach can also be easily adapted to a high-throughput platform for biological and drug discovery applications.

Acknowledgements

This research has been funded by the US Army Engineer Research and Development Center, the Institute for Soldier Nanotechnology, NIH, the Coulter Foundation and the Draper Laboratory. We would like to thank Drs. Utkan Demirci, Young Song, Won Gu Lee, Edward Haeggstrom and Ms. Tracy Chang for the scientific and technical support. This research was supported in part by an appointment to the postgraduate research participation program at the US Army Engineer Research and Development Center, Construction Engineering Research Laboratory (ERDC-CERL), administered by the Oak Ridge Institute for Science and Education.

References

1 N. Li Jeon, H. Baskaran, S. K. Dertinger, G. M. Whitesides, L. Van de Water and M. Toner, *Nat. Biotechnol.*, 2002, **20**, 826–830.
2 A. Khademhosseini, R. Langer, J. Borenstein and J. P. Vacanti, *Proc. Natl. Acad. Sci. U. S. A.*, 2006, **103**, 2480–2487.
3 A. Shamloo, N. Ma, M. M. Poo, L. L. Sohn and S. C. Heilshorn, *Lab Chip*, 2008, **8**, 1292–1299.
4 B. G. Chung, F. Lin and N. L. Jeon, *Lab Chip*, 2006, 6764–768.
5 J. Pihl, J. Sinclair, E. Sahlin, M. Karlsson, F. Petterson, J. Olofsson and O. Orwar, *Anal. Chem.*, 2005, **77**, 3897–3903.
6 B. G. Chung, L. A. Flanagan, S. W. Rhee, P. H. Schwartz, A. P. Lee, E. S. Monuki and N. L. Jeon, *Lab Chip*, 2005, **5**, 401–406.
7 M. Yang, J. Yang, C. W. Li and J. Zhao, *Lab Chip*, 2002, **2**, 158–163.
8 T. M. Keenan and A. Folch, *Lab Chip*, 2008, **8**, 34–57.
9 S. K. W. Dertinger, D. T. Chiu, N. L. Jeon and G. M. Whitesides, *Anal. Chem.*, 2001, **73**, 1240–1246.
10 M. A. Holden, S. Kumar, E. T. Castellana, A. Beskok and P. S. Cremer, *Sens. Actuators, B*, 2003, **92**, 199–207.
11 E. A. Schilling, A. E. Kamholz and P. Yager, *Anal. Chem.*, 2002, **74**, 1798–1804.
12 F. I. Rustem, D. S. Abraham, J. A. K. Paul, W. George and A. S. Howard, *Appl. Phys. Lett.*, 2000, **76**, 2376–2378.
13 B. R. Gorman and J. P. Wikswo, *Microfluid. Nanofluid.*, 2008, **4**, 273–285.
14 B. Mosadegh, C. Huang, J. W. Park, H. S. Shin, B. G. Chung, S. K. Hwang, K. H. Lee, H. J. Kim, J. Brody and N. L. Jeon, *Langmuir*, 2007, **23**, 10910–10912.
15 V. V. Abhyankar, M. A. Lokuta, A. Huttenlocher and D. J. Beebe, *Lab Chip*, 2006, **6**, 389–393.
16 I. Meyvantsson, J. W. Warrick, S. Hayes, A. Skoien and D. J. Beebe, *Lab Chip*, 2008, **8**, 717–724.
17 H. Wu, B. Huang and R. N. Zare, *J. Am. Chem. Soc.*, 2006, **128**, 4194–4195.
18 J. Goulpeau, B. Lonetti, D. Trouchet, A. Ajdari and P. Tabeling, *Lab Chip*, 2007, **7**, 1154–1161.
19 T. Kang, J. Han and K. S. Lee, *Lab Chip*, 2008, **8**, 1220–1222.
20 G. M. Walker and D. J. Beebe, *Lab Chip*, 2002, **2**, 131–134.
21 E. Berthier, J. Warrick, H. Yu and D. J. Beebe, *Lab Chip*, 2008, **8**, 860–864.
22 E. Berthier, J. Warrick, H. Yu and D. J. Beebe, *Lab Chip*, 2008, **8**, 852–859.
23 N. Goedecke, J. Eijkel and A. Manz, *Lab Chip*, 2002, **2**, 219–223.
24 W. Wang, J. Lin and D. C. Schwartz, *Biophys. J.*, 1998, **75**, 513–520.
25 G. M. Walker and D. J. Beebe, *Lab Chip*, 2002, **2**, 57–61.
26 G. C. Randall and P. S. Doyle, *Proc. Natl. Acad. Sci. U. S. A.*, 2005, **102**, 10813–10818.
27 F. M. White, *Viscous Fluid Flow*, 2nd edn, McGraw-Hill, New York, 1991.
28 G. I. Taylor, *Proc. R. Soc. London, Ser. A*, 1953, **219**, 186–203.
29 G. I. Taylor, *Proc. R. Soc. London, Ser. A*, 1954, **225**, 473–477.
30 R. Aris, *Proc. R. Soc. London, Ser. A*, 1956, **235**, 67–77.
31 M. R. Doshi, P. M. Daiya and W. N. Gill, *Chem. Eng. Sci.*, 1979, **33**, 795–804.
32 P. C. Chatwin and P. J. Sullivan, *J. Fluid Mech.*, 1982, **120**, 347–358.
33 W. C. Claycomb, N. A. Lanson, Jr., B. S. Stallworth, D. B. Egeland, J. B. Delcarpio, A. Bahinski and N. J. Izzo, Jr., *Proc. Natl. Acad. Sci. U. S. A.*, 1998, **95**, 2979–2984.
34 A. Natarajan, P. Molnar, K. Sieverdes, A. Jamshidi and J. J. Hickman, *Toxicol. in Vitro*, 2006, **20**, 375–381.